

Geometry-Aware Uncertainty Coresets for Robust Visual In-Context Learning in Histopathology

Franciskus Xaverius Erick¹, Johanna Paula Müller¹, and
Bernhard Kainz^{1,2}

¹ FAU Erlangen-Nürnberg, Erlangen, DE
`franciskus.erick@fau.de`

² Department of Computing, Imperial College London, London, UK

Abstract. Vision-language models (VLMs) can couple visual perception with open-ended clinical reasoning, making them attractive for computational histopathology. However, fine-tuning billions of parameters on scarce, expert-annotated pathology data is prohibitive, while in-context learning (ICL), which conditions the VLM on demonstrative image-text pairs without parameter updates, suffers from high sensitivity to which examples are selected and how the query is phrased, producing unreliable diagnostics. Existing selection strategies rely on query-dependent nearest-neighbour retrieval that ignores global data structure, require costly parameter updates, or disregard the joint vision-text embedding geometry of VLMs. We propose GAUC, a training-free coreset selection method operating directly in the pre-trained multimodal embedding space. GAUC jointly optimises three objectives: (1) a Maximum Mean Discrepancy term enforcing distributional fidelity between coreset and full dataset, (2) an Effective Mutual Information Difference regulariser bounding performance degradation under prompt paraphrases by exploiting the VLM’s joint vision-text alignment, and (3) a predictive-variance penalty suppressing overconfident, unstable outputs. On CRC-100K and MHIST across multiple open-source VLM architectures, GAUC consistently improves accuracy, calibration, and prompt robustness over recent ICL selection methods and dataset-distillation baselines, all without a single gradient update. Code is available at [Github Repository](#)

Keywords: Vision-Language Model · Coreset Selection · In-Context Learning · Uncertainty.

1 Introduction

Histopathological examination remains the diagnostic gold standard for most solid tumours, requiring trained pathologists to visually assess tissue morphology at high magnification, a process that is time-consuming, subjective, and bottlenecked by a global shortage of specialist expertise [5]. With colorectal cancer alone accounting for over 1.9 million new cases and 935,000 deaths annually [10], scalable tools that support high-throughput tissue classification are needed. The

widespread adoption of automated sample preparation pipelines and whole-slide image (WSI) scanners has further intensified this demand by dramatically accelerating the rate at which digitised histology data is generated, placing mounting workload pressure on pathologists [5]. Pre-trained vision-language models (VLMs) offer a compelling path forward: by coupling a vision encoder with a large language backbone, they interpret complex medical imagery while producing human-readable diagnostic rationales that mirror clinician reasoning [16,14]. Unlike conventional supervised classifiers, VLMs can simultaneously process visual evidence and contextual clinical descriptions, enabling more holistic and interpretable tissue analysis [9].

However, deploying VLMs clinically is hindered by the intractability of fine-tuning billions of parameters on scarce, privacy-sensitive data [14] and by persistent overconfident hallucinations that are unacceptable in safety-critical settings [22,4]. In-context learning (ICL) sidesteps the first obstacle by conditioning the model on demonstrative image-label pairs placed directly in the prompt, requiring no parameter updates [3]. This capability, originally observed in large language models, transfers naturally to VLMs [1,2,15]. Yet ICL is notoriously sensitive to both the choice of demonstrations and the phrasing of the textual query [19,29,17]. Current remedies either insert learnable shift modules that require additional training [12,17], or rely on nearest-neighbour retrieval that captures local query similarity but ignores the global distributional structure of the dataset [9]. Neither accounts for the joint visual-textual embedding geometry of the VLM, nor explicitly controls for prompt-induced instability or predictive overconfidence, shortcomings that are especially damaging in histopathology where class imbalance obscures minority morphologies and minor prompt reformulations can flip a diagnosis. We propose a principled, entirely training-free coreset selection framework for visual ICL that jointly optimises representativeness, prompt robustness, and predictive calibration. Our contributions are:

1. A geometry-aware objective based on Maximum Mean Discrepancy (MMD) that selects real, clinically traceable demonstrations whose embedding distribution preserves the global structure of the full dataset, preventing collapse into dominant morphological clusters.
2. An Effective Mutual Information Difference (EMID)-derived mutual-information regulariser that quantifies response discrepancies under paraphrased queries, steering selection toward in-context sets robust to textual variation across both visual and textual modality embeddings.
3. A variance regularisation term that penalises predictive uncertainty, encouraging demonstrations that minimise output entropy and suppress overconfident hallucinations.
4. Consistent improvements over nearest-neighbour and random baselines on two challenging histopathology benchmarks, CRC-100K (8-class tissue subtyping) and MHIST (binary polyp classification), with fully training-free deployment compatible with any off-the-shelf VLM.

Related Work. Recent works in ICL [18] have formalised demonstrations as latent shift vectors that steer query-token representations, and extended this view

to multimodal models through lightweight query-dependent shift modules [12] and prompt-configuration strategies [17]. These methods are effective but require learnable parameters or task-specific inference modifications. In computational pathology, k -Nearest Neighbour (k NN) retrieval of demonstration images has matched or exceeded specialised fine-tuned networks [9], yet k NN selects solely by local query proximity. Two broader strategies exist for constructing representative subsets: dataset distillation synthesises artificial samples by matching gradient trajectories, feature distributions, or diffusion-based latent mappings [28, 8, 7] but is computationally expensive and produces clinically untraceable images, whereas coreset selection retrieves real samples and can enforce distributional fidelity through statistical distances such as Maximum Mean Discrepancy [25]. Curriculum-based adaptation on biomedical figure-caption corpora effectively aligns VLM semantics with visual features [16], yet clinical VLMs remain prone to overconfident hallucinations and prompt-induced output instability [22, 4, 14]. The Effective Mutual Information Difference (EMID) upper-bounds the performance degradation from multimodal alignment shifts via Jensen-Shannon divergence in the joint latent space [21]. The quality of any geometry-aware selection further depends on the feature space; self-supervised Vision Transformers pre-trained on histopathology data through masked image modelling [11] provide the semantically rich embeddings required for distributional metrics to reflect genuine morphological variation.

2 Method

Let W_θ denote a pre-trained VLM with frozen parameters θ . Given a full labelled dataset $F = \{(x_i, y_i)\}_{i=1}^{|F|}$ of histopathology patches and their class labels, we seek a compact coreset $\mathcal{D} = \{(x_j, y_j)\}_{j=1}^{|\mathcal{D}|}$ with $|\mathcal{D}| \ll |F|$ that, when placed in the prompt as in-context demonstrations, maximises diagnostic accuracy while remaining robust to prompt variation and predictive overconfidence. We optimise \mathcal{D} by minimising a composite objective over three complementary terms (Fig. 1), each operating entirely in the pre-trained embedding space of W_θ without any gradient-based parameter updates.

Geometry-aware coreset selection via MMD. We require the embedding distribution of \mathcal{D} to faithfully mirror that of F . Let x, x' denote independent samples from F and u, u' from \mathcal{D} , mapped through the vision encoder of W_θ . We measure distributional discrepancy with the Maximum Mean Discrepancy in a reproducing kernel Hilbert space [23]:

$$\text{MMD}^2(F, \mathcal{D}) = \mathbb{E}_{x, x'}[k(x, x')] + \mathbb{E}_{u, u'}[k(u, u')] - 2\mathbb{E}_{x, u}[k(x, u)], \quad (1)$$

where $k(x, u) = \exp(-\|x - u\|^2/2\sigma^2)$ is the RBF kernel. Minimising MMD^2 enforces a geometric constraint that prevents the coreset from collapsing into locally dominant clusters and ensures global representativeness across all tissue morphologies.

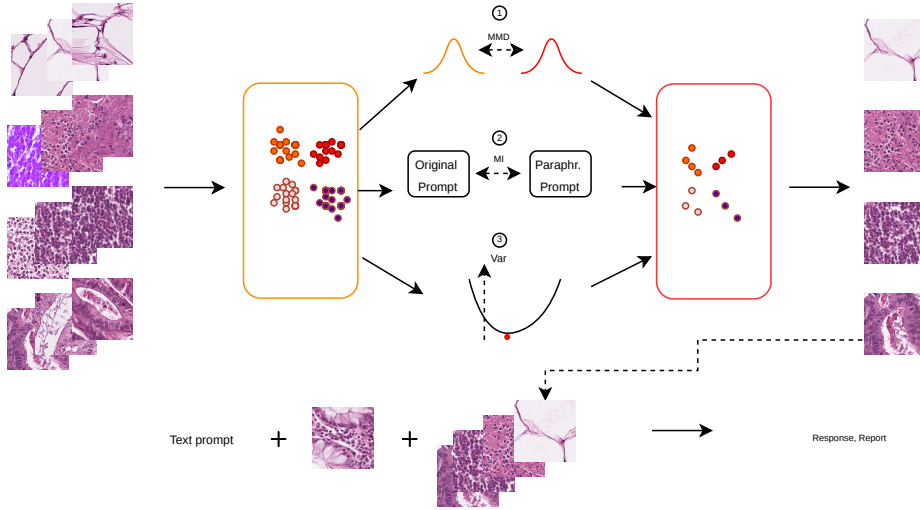


Fig. 1: The GAUC optimization pipeline. GAUC involves 1) MMD matching between the embedded distribution of the full dataset and the selected coreset examples, 2) effective mutual information upper bound regularisation between outputs with original text prompts and paraphrased prompts, and 3) variance uncertainty minimisation of selected coreset examples.

Prompt-robustness regularisation via EMID. Minor textual rephrasing of the query prompt can shift the conditional response distribution of a VLM, degrading diagnostic reliability. We regularise against this instability using EMID [21]. For a query image x , coreset \mathcal{D} , original prompt t , and paraphrased variant t' , the mutual information between the model response r and the multimodal input is $I(r; x, \mathcal{D}, t) = H(r) - H(r | x, \mathcal{D}, t)$. The EMID quantifies how this coupling degrades under the prompt shift $t \rightarrow t'$: $\text{EMID}(P, Q) = \text{EMI}(P(r | x, \mathcal{D}, t)) - \text{EMI}(Q(r' | x, \mathcal{D}, t'))$, where P and Q denote the response distributions under the original and paraphrased prompts. A tractable upper bound decomposes into Jensen-Shannon divergences over the individual modality embeddings:

$$\text{EMID}_{\text{upper}} = D_{JS}^{1/2}(P_x \| Q_x) + D_{JS}^{1/2}(P_t \| Q_t) + D_{JS}^{1/4}(P_{\hat{r}} \| P_r) + D_{JS}^{1/4}(P_{\hat{r}} \| Q_{r'}), \quad (2)$$

where P_x, Q_x and P_t, Q_t are the visual and textual embedding distributions under each prompt, $P_r, Q_{r'}$ the corresponding response distributions, and \hat{r} the ideal ground-truth response. We treat prompt paraphrases, generated by a separate LLM, as localised distribution shifts in the textual modality and penalise coresets that yield large $\text{EMID}_{\text{upper}}$. Unlike retrieval methods that operate solely on image embeddings [25], this term explicitly leverages the joint vision-text alignment of the VLM to enforce prompt invariance.

Predictive variance regularisation. To suppress overconfident yet unstable predictions, we penalise the variance of the model’s output distribution across

class labels. For a classification task with label set \mathcal{Y} , we define $\text{Var}(\mathcal{D}) = \text{Var}_{k \in \mathcal{Y}}[\log p(y_k | x, \mathcal{D})]$, where $p(y_k | x, \mathcal{D})$ is the predicted probability for class k given the query and the coreset. Minimising this term steers the selection toward demonstrations that yield concentrated, low-entropy predictive distributions, discouraging coresets that leave the model ambivalent or overconfident on incorrect classes.

Joint objective. The final coreset is obtained by jointly minimising:

$$\mathcal{D}^* = \arg \min_{\mathcal{D}} \text{MMD}^2(F, \mathcal{D}) + \alpha \text{EMID}_{\text{upper}} + \beta \text{Var}(\mathcal{D}), \quad (3)$$

with $\alpha, \beta \geq 0$ controlling the trade-off between distributional fidelity, prompt robustness, and predictive stability. Because all three terms are evaluated from forward-pass embeddings and output log-probabilities, the entire optimisation is training-free, requires no backward passes through W_θ , and produces a single query-independent coreset reusable across all test images.

3 Experiments

We evaluate on two histopathology benchmarks. **CRC-100K** [13] contains 100,000 H&E-stained colorectal tissue patches spanning 9 classes; following prior work [9,11,24] we omit the background class and report 8-class performance. **MHIST** [26] consists of 3,152 colorectal polyp patches annotated as hyperplastic polyp (HP) or sessile serrated adenoma (SSA), a binary task that is challenging even for trained pathologists. All experiments use two open-source VLM families, Qwen and LLaVA, loaded with default ImageNet pre-trained weights from HuggingFace to test out-of-domain ICL capability. We optimise coresets via greedy selection for 1,000 iterations with $\alpha = 0.1$, $\beta = 0.1$ in Eq. 3.

Baselines. We compare against three ICL demonstration-selection strategies: random sampling, k NN retrieval [9], and mutual-information-informed retrieval (DR) [25], as well as the shift-vector method MIMIC [12] which requires additional training. We further include three dataset-distillation baselines: Trajectory Matching (TM) [6], Distribution Matching (DM) [27], and diffusion-based distillation (D3R) [28].

Statistical testing. To assess whether observed differences are statistically meaningful, we apply the two-sided Wilcoxon signed-rank test over paired per-run metric values between GAUC and each baseline. This non-parametric test is appropriate given the moderate number of runs and makes no distributional assumptions on the metric differences. We report significance at $p < 0.05$ (†) and $p < 0.01$ (‡) in all tables.

Classification and calibration (Tables 1, 2). On CRC-100K with Qwen at 3-shot, GAUC achieves the highest accuracy ($0.610_{\pm 0.030}$) and F1 ($0.588_{\pm 0.015}$), improving over the strongest, heavyweight learned baseline MIMIC by 1.16 percentage points ($p < 0.05$, Wilcoxon signed-rank) while simultaneously reducing ECE over the mutual-information aligned dual retrieval (DR) baseline from $0.153_{\pm 0.015}$ to $0.145_{\pm 0.012}$, indicating substantially better-calibrated predictions. The gains are consistent across models: with LLaVA, GAUC yields the

Table 1: Classification and calibration on **CRC-100K** (8-class). Best in **bold**, second-best underlined. †/‡: GAUC significantly better than the best baseline at $p < 0.05$ / $p < 0.01$ (Wilcoxon signed-rank, 10 runs).

Model Method	1-shot				3-shot				
	Acc \uparrow	F1 \uparrow	NLL \downarrow	ECE \downarrow	Acc \uparrow	F1 \uparrow	NLL \downarrow	ECE \downarrow	
Qwen	Random	0.334 \pm 0.082	0.207 \pm 0.032	5.047 \pm 0.110	0.513 \pm 0.028	0.401 \pm 0.064	0.374 \pm 0.024	4.923 \pm 0.095	0.340 \pm 0.021
	kNN	0.402 \pm 0.067	0.366 \pm 0.027	4.951 \pm 0.090	0.387 \pm 0.022	0.593 \pm 0.051	0.557 \pm 0.019	4.877 \pm 0.082	0.156 \pm 0.016
	DR	0.390 \pm 0.069	<u>0.367</u> \pm 0.026	<u>4.832</u> \pm 0.085	<u>0.310</u> \pm 0.020	0.591 \pm 0.049	0.562 \pm 0.018	<u>4.765</u> \pm 0.075	<u>0.153</u> \pm 0.015
	TM	0.175 \pm 0.056	0.158 \pm 0.024	6.103 \pm 0.120	0.506 \pm 0.030	0.217 \pm 0.044	0.185 \pm 0.020	5.887 \pm 0.105	0.308 \pm 0.020
	DM	0.123 \pm 0.051	0.119 \pm 0.022	5.986 \pm 0.115	0.555 \pm 0.032	0.204 \pm 0.041	0.178 \pm 0.019	5.971 \pm 0.100	0.379 \pm 0.023
	D3R	0.217 \pm 0.058	0.191 \pm 0.025	5.088 \pm 0.095	0.483 \pm 0.026	0.395 \pm 0.048	0.186 \pm 0.021	4.996 \pm 0.085	0.335 \pm 0.020
	MIMIC	0.325 \pm 0.047	0.341 \pm 0.028	4.993 \pm 0.088	0.422 \pm 0.024	<u>0.603</u> \pm 0.035	<u>0.583</u> \pm 0.016	4.779 \pm 0.072	0.188 \pm 0.016
	GAUC (ours)	<u>0.398</u> \pm 0.038	0.370 \pm 0.024	4.788 \pm 0.080	0.308 \pm 0.018	0.610 \pm 0.030	0.588 \pm 0.015	4.592 \pm 0.065	0.145 \pm 0.012
	LLaVA	Random	0.281 \pm 0.087	0.146 \pm 0.038	5.382 \pm 0.125	0.442 \pm 0.030	0.360 \pm 0.067	0.343 \pm 0.029	5.186 \pm 0.110
kNN		<u>0.338</u> \pm 0.079	0.312 \pm 0.034	5.170 \pm 0.105	0.405 \pm 0.026	<u>0.503</u> \pm 0.055	0.469 \pm 0.024	5.034 \pm 0.095	0.287 \pm 0.019
DR		0.350 \pm 0.077	<u>0.320</u> \pm 0.033	4.968 \pm 0.100	<u>0.372</u> \pm 0.024	0.495 \pm 0.052	0.463 \pm 0.025	4.883 \pm 0.088	0.256 \pm 0.018
TM		0.164 \pm 0.061	0.128 \pm 0.027	6.085 \pm 0.130	0.525 \pm 0.032	0.323 \pm 0.050	0.295 \pm 0.022	5.978 \pm 0.115	0.423 \pm 0.025
DM		0.156 \pm 0.059	0.120 \pm 0.026	5.983 \pm 0.120	0.530 \pm 0.033	0.301 \pm 0.047	0.279 \pm 0.021	5.991 \pm 0.108	0.438 \pm 0.026
D3R		0.183 \pm 0.063	0.165 \pm 0.029	5.522 \pm 0.110	0.473 \pm 0.028	0.343 \pm 0.051	0.330 \pm 0.023	5.400 \pm 0.098	0.365 \pm 0.021
MIMIC		0.307 \pm 0.060	0.281 \pm 0.031	<u>4.882</u> \pm 0.090	0.383 \pm 0.023	0.507 \pm 0.044	<u>0.471</u> \pm 0.020	<u>4.805</u> \pm 0.082	<u>0.248</u> \pm 0.017
GAUC (ours)		0.335 \pm 0.053	0.323 \pm 0.030	4.810 \pm 0.085	0.346 \pm 0.021	0.498 \pm 0.042	0.485 \pm 0.019	4.723 \pm 0.075	0.204 \pm 0.015

best F1 in both shot regimes and reduces ECE by 0.044 absolute points over the next-best method, with all pairwise improvements over kNN and MIMIC reaching significance at $p < 0.01$. Dataset-distillation baselines (TM, DM, D3R) perform markedly worse across all metrics ($p < 0.01$ in all comparisons), confirming that synthetic demonstrations are poorly suited for VLM-based ICL in histopathology. On MHIST (Table 2), GAUC achieves 0.652 \pm 0.012 $_X$ accuracy at 3-shot with Qwen, outperforming kNN (0.645 \pm 0.015) by 0.007 points ($p < 0.05$). GAUC achieves comparable 1-shot and 3-shot accuracies for different models and datasets to the baselines, while achieving considerable improvements in F1, NLL, and ECE, indicating robustness without sacrificing accuracy.

Robustness to prompt variation and hallucinations (Table 3). GAUC yields the lowest Var-para across both models and shot settings ($p < 0.01$ vs. all baselines), confirming that the EMID regulariser (Eq. 2) effectively suppresses sensitivity to prompt paraphrasing. Var-runs is likewise reduced, indicating that the selected coresets produce stable predictions across independent evaluations rather than relying on fortunate random seeds. On the hallucination metrics, GAUC achieves 0.795 \pm 0.014 CHAIRs and 0.539 \pm 0.007 CHAIRi at 3-shot with Qwen, representing a 1.61% relative reduction over MIMIC ($p < 0.05$). This confirms that the variance penalty in Eq. 3 discourages demonstration sets that leave the model in high-entropy states where hallucinated findings are more likely.

Qualitative analysis (Fig. 2). We visualise the demonstrations selected by kNN and GAUC for the same query. The kNN coreset clusters around a single morphological pattern, offering the VLM a narrow distributional view that triggers a confident misclassification. GAUC instead selects demonstrations spanning multiple tissue classes, providing the geometric diversity enforced by the MMD term (Eq. 1). The resulting prediction is correct and better calibrated,

Table 2: Classification and calibration on **MHIST** (binary). Best in **bold**, second-best underlined. †/‡: GAUC significantly better than the best baseline at $p < 0.05/p < 0.01$ (Wilcoxon signed-rank, 10 runs).

Model Method	1-shot				3-shot				
	Acc↑	F1↑	NLL↓	ECE↓	Acc↑	F1↑	NLL↓	ECE↓	
Qwen	Random	0.554±0.018	0.537±0.020	4.865±0.045	0.193±0.012	0.627±0.016	0.608±0.018	4.792±0.038	0.126±0.010
	kNN	0.560 ±0.017	0.542 ±0.019	<u>4.802</u> ±0.042	0.188 ±0.011	<u>0.645</u> ±0.015	0.624±0.016	4.517±0.036	0.102±0.008
	DR	<u>0.558</u> ±0.016	0.543 ±0.018	4.877±0.043	0.198±0.010	0.636±0.014	0.625±0.015	4.590±0.034	<u>0.086</u> ±0.007
	TM	0.352±0.012	0.336±0.013	5.016±0.048	0.229±0.014	0.524±0.010	0.503±0.012	4.933±0.040	0.205±0.011
	DM	0.348±0.011	0.328±0.013	5.110±0.049	0.243±0.013	0.511±0.010	0.499±0.011	5.005±0.042	0.218±0.012
	D3R	0.548±0.017	0.537±0.018	4.923±0.044	0.208±0.012	0.619±0.015	0.600±0.016	4.559±0.037	0.133±0.010
	MIMIC	0.531±0.016	0.514±0.017	4.875±0.043	0.201±0.011	<u>0.649</u> ±0.014	<u>0.637</u> ±0.015	<u>4.502</u> ±0.034	0.098±0.007
	GAUC (ours)	0.549±0.014	0.539±0.013	4.808 ±0.020	<u>0.190</u> ±0.011	0.652 ±0.012	0.640 ±0.011	4.433 ±0.018	0.073 ±0.007
LLaVA	Random	0.538±0.018	0.512±0.020	4.926±0.045	0.278±0.014	0.598±0.016	0.563±0.018	4.860±0.038	0.185±0.012
	kNN	0.546 ±0.017	0.519±0.018	4.907±0.043	<u>0.262</u> ±0.013	0.611±0.015	0.583±0.016	4.783±0.036	0.153±0.010
	DR	0.523±0.016	0.506±0.017	4.832 ±0.042	0.282±0.013	0.603±0.014	<u>0.589</u> ±0.015	4.702±0.034	<u>0.144</u> ±0.009
	TM	0.341±0.012	0.308±0.013	5.325±0.052	0.313±0.015	0.446±0.010	0.410±0.012	5.296±0.045	0.276±0.012
	DM	0.329±0.011	0.294±0.012	5.290±0.051	0.335±0.014	0.439±0.010	0.408±0.011	5.339±0.045	0.291±0.013
	D3R	0.509±0.016	0.487±0.017	4.914±0.043	0.284±0.012	0.587±0.015	0.555±0.016	4.937±0.036	0.199±0.010
	MIMIC	0.535±0.017	0.503±0.018	4.911±0.043	0.273±0.012	0.618 ±0.015	0.584±0.016	4.805±0.036	0.162±0.010
	GAUC (ours)	<u>0.540</u> ±0.014	0.528 ±0.012	<u>4.883</u> ±0.020	0.288 ±0.010	<u>0.609</u> ±0.012	0.592 ±0.011	4.684 ±0.017	0.130 ±0.008

Table 3: Robustness and hallucination evaluation on **CRC-100K**. Var-para/Var-runs: prediction variance under prompt paraphrases / across independent runs (lower = more stable). CHAIRs/CHAIRi: sentence-/instance-level hallucination rates (lower = fewer fabricated findings). Notation as in Table 1.

Model Method	1-shot				3-shot				
	Var-para↓	Var-runs↓	CHAIRs↓	CHAIRi↓	Var-para↓	Var-runs↓	CHAIRs↓	CHAIRi↓	
Qwen	Random	0.283±0.012	0.227	0.916±0.020	0.640±0.015	0.265±0.011	0.187	0.912±0.019	0.633±0.014
	kNN	0.207±0.010	0.183	0.852±0.018	0.585±0.012	0.197±0.009	0.125	0.847±0.017	0.579±0.011
	DR	0.210±0.011	0.190	0.841±0.017	0.577±0.011	0.190±0.009	<u>0.120</u>	0.829±0.016	0.565±0.010
	MIMIC	<u>0.175</u> ±0.009	<u>0.145</u>	0.819±0.016	<u>0.560</u> ±0.009	<u>0.163</u> ±0.007	0.107	<u>0.808</u> ±0.015	<u>0.548</u> ±0.008
	GAUC (ours)	0.127 ±0.007	0.103 †	0.803 ±0.015	0.552 ±0.008	0.105 ±0.006	0.095 †	0.795 ±0.014	0.539 ±0.007
	LLaVA	Random	0.310±0.013	0.255	1.019±0.021	0.732±0.016	0.297±0.012	0.213	0.996±0.020
kNN		0.233±0.011	0.230	0.994±0.020	0.700±0.014	0.213±0.010	0.175	0.983±0.019	0.681±0.012
DR		<u>0.215</u> ±0.010	0.223	0.990±0.019	0.706±0.013	<u>0.200</u> ±0.009	0.190	0.987±0.018	0.678±0.011
MIMIC		0.220±0.010	<u>0.187</u>	0.938 ±0.017	<u>0.637</u> ±0.010	0.197±0.009	<u>0.147</u>	0.925 ±0.016	<u>0.614</u> ±0.009
GAUC (ours)		0.207 ±0.008	0.163 †	<u>0.943</u> ±0.016	0.630 ±0.008	0.190 ±0.007	0.130 †	<u>0.936</u> ±0.015	0.608 ±0.007

with the model assigning 81.3% confidence to the true class compared to 39.7% under k NN.

Ablation (Table 4). Removing the EMID regulariser ($\alpha=0$) increases Var-para by 74.28% ($p < 0.01$), confirming its role in prompt robustness, while accuracy drops by 0.007 points. Dropping variance regularisation ($\beta=0$) degrades ECE from 0.145 ± 0.012 to 0.165 ± 0.015 ($p < 0.01$), demonstrating its contribution to calibration. Using MMD alone ($\alpha=\beta=0$) still outperforms k NN and random baselines significantly ($p < 0.01$), validating the geometric term as a strong standalone objective, but underperforms the full model on all metrics. All three terms contribute complementary, statistically significant gains; the full objective achieves the best trade-off across accuracy, calibration, and robustness.

Discussion. Our optimization of Eq. 3 scales linearly in the number of candidate samples and requires only forward-pass embeddings, making it practical even

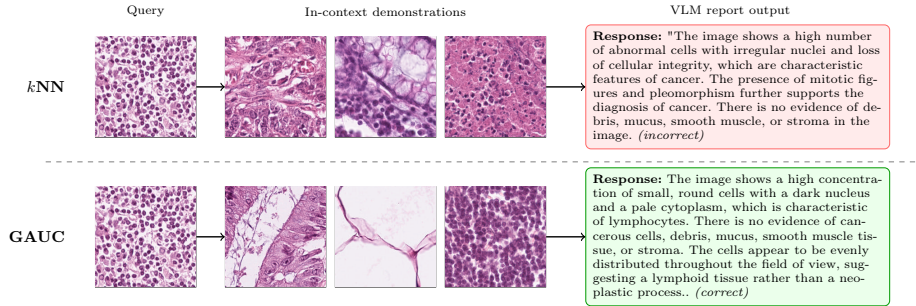


Fig. 2: Qualitative comparison. **Top:** k NN selects morphologically redundant demonstrations, leading to a misclassification. **Bottom:** GAUC provides diverse, globally representative demonstrations yielding the correct diagnosis.

Table 4: Ablation on **CRC-100K** (3-shot, Qwen). Each row removes one term from Eq. 3. †/‡: full model significantly better at $p<0.05$ / $p<0.01$.

Variant	Acc \uparrow	F1 \uparrow	ECE \downarrow	Var-para \downarrow	Var-runs \downarrow
GAUC (full)	0.610 ± 0.030 [†]	0.588 ± 0.015 [†]	0.145 ± 0.012 [‡]	0.105 ± 0.006 [‡]	0.095 [†]
w/o EMID ($\alpha=0$)	0.603 ± 0.035	0.579 ± 0.022	0.150 ± 0.014	0.183 ± 0.010	0.098
w/o Var ($\beta=0$)	0.597 ± 0.037	0.563 ± 0.021	0.165 ± 0.015	0.111 ± 0.007	0.117
MMD only ($\alpha=\beta=0$)	0.600 ± 0.036	0.559 ± 0.023	0.172 ± 0.016	0.186 ± 0.009	0.113

on a single GPU. Because the coreset is selected once and reused across all queries, the per-inference cost is identical to standard ICL with no additional overhead. The current formulation assumes access to a class-balanced candidate pool; in settings with severe class imbalance, a stratified sampling stage prior to optimisation could further improve minority-class coverage. We also note that the EMID upper bound relies on Gaussian approximations of the embedding distributions, which may loosen for highly multimodal feature spaces. Tighter variational bounds or sample-based estimators could be explored in future work.

4 Conclusion

We presented GAUC, a training-free coreset selection method that makes visual in-context learning reliable enough for clinical histopathology. By jointly optimizing distributional fidelity (MMD), prompt robustness (EMID), and predictive stability (variance regularization) directly in the pre-trained multimodal embedding space, GAUC selects real, clinically traceable demonstration images that consistently improve accuracy, calibration, and robustness to prompt variation across two VLM architectures and two challenging benchmarks. We believe this principled integration of geometry-aware selection with information-theoretic prompt invariance establishes a new standard for trustworthy, training-free diagnostic support in computational pathology and generalities naturally to other safety-critical domains where reliable in-context can be useful.

Acknowledgments. We acknowledge HPC resources from NHR@FAU (projects b143dc, b180dc), funded by federal and Bavarian state authorities and Gerhard Wellein’s HPC approach. NHR@FAU hardware is partially funded by DFG 440719683. Additional support was received from ERC projects MIA-NORMAL 101083647, DFG 513220538 and 512819079, and the state of Bavaria (HTA and the Bavarian Foundation Model Initiative). We further acknowledge resources provided by the Isambard-AI National AI Research Resource (AIRR), operated by the University of Bristol and funded by DSIT via UKRI and STFC [ST/AIRR/I-A-I/1023] [20]. We were supported by coding agents and LLMs from Anthropic, OpenAI, Google, and Mistral AI, for text polishing, coding, experiment orchestration, and cluster monitoring.

Disclosure of Interests. The authors have no relevant competing interests.

References

1. Achiam, J., et al.: GPT-4 technical report. Tech. rep., OpenAI (2024), arXiv:2303.08774
2. Awadalla, A., Gao, I., Gardner, J., Hessel, J., Hanafy, Y., Zhu, W., Marathe, K., Bitton, Y., Gadre, S., Sagawa, S., Jitsev, J., Kornblith, S., Koh, P.W., Ilharco, G., Wortsman, M., Schmidt, L.: OpenFlamingo: An open-source framework for training large autoregressive vision-language models (2023), arXiv:2308.01390
3. Brown, T.B., Mann, B., Ryder, N., Subbiah, M., Kaplan, J., Dhariwal, P., Neelakantan, A., Shyam, P., Sastry, G., Askell, A., Agarwal, S., Herbert-Voss, A., Krueger, G., Henighan, T., Child, R., Ramesh, A., Ziegler, D.M., Wu, J., Winter, C., Hesse, C., Chen, M., Sigler, E., Litwin, M., Gray, S., Chess, B., Clark, J., Berner, C., McCandlish, S., Radford, A., Sutskever, I., Amodei, D.: Language models are few-shot learners. In: NeurIPS’20. vol. 33, pp. 1877–1901 (2020)
4. Bungert, T.J., Kobelke, L., Jaeger, P.F.: Understanding silent failures in medical image classification. In: MICCAI’23. pp. 400–410 (2023)
5. Campanella, G., Hanna, M.G., Geneslaw, L., Miraflor, A., Silva, V.W.K., Busam, K.J., Brogi, E., Reuter, V.E., Klimstra, D.S., Fuchs, T.J.: Clinical-grade computational pathology using weakly supervised deep learning on whole slide images. *Nature Medicine* **25**(8), 1301–1309 (2019). <https://doi.org/10.1038/s41591-019-0508-1>
6. Cazenavette, G., Wang, T., Torralba, A., Efros, A.A., Zhu, J.Y.: Dataset distillation by matching training trajectories. In: CVPR’22. pp. 4750–4759 (2022)
7. Cechnicka, S., Ball, J., Baugh, M., Reynaud, H., Simmonds, N., Smith, A.P., Horsfield, C., Roufosse, C., Kainz, B.: URCDM: Ultra-resolution image synthesis in histopathology. In: MICCAI’24. pp. 535–545 (2024)
8. Cechnicka, S., Ball, J., Reynaud, H., Arthurs, C., Roufosse, C., Kainz, B.: Realistic data enrichment for robust image segmentation in histopathology. In: MICCAI’23 Workshop on Domain Adaptation and Representation Transfer. pp. 63–72 (2023)
9. Ferber, D., Wölflein, G., Wiest, I.C., Ligerio, M., Sainath, S., Ghaffari Laleh, N., El Nahhas, O.S.M., Müller-Franzes, G., Jäger, D., Truhn, D., Kather, J.N.: In-context learning enables multimodal large language models to classify cancer pathology images. *Nature Communications* **15**(1), 10104 (2024). <https://doi.org/10.1038/s41467-024-51465-9>
10. Ferlay, J., Colombet, M., Soerjomataram, I., Parkin, D.M., Piñeros, M., Znaor, A., Bray, F.: Cancer statistics for the year 2020: An overview. *International Journal*

- of Cancer **149**(4), 778–789 (2021). <https://doi.org/https://doi.org/10.1002/ijc.33588>, <https://onlinelibrary.wiley.com/doi/abs/10.1002/ijc.33588>
11. Filiot, A., Ghermi, R., Olivier, A., Jacob, P., Fidon, L., Camara, A., Mac Kain, A., Saillard, C., Schiratti, J.B.: Scaling self-supervised learning for histopathology with masked image modeling. medRxiv (2023). <https://doi.org/10.1101/2023.07.21.23292757>
 12. Jiang, Y., Fu, J., Hao, C., Hu, X., Peng, Y., Geng, X., Yang, X.: Mimic in-context learning for multimodal tasks. In: CVPR'25. pp. 29825–29834 (2025)
 13. Kather, J.N., Krisam, J., Charoentong, P., Luedde, T., Herpel, E., Weis, C.A., Gaiser, T., Marx, A., Valous, N.A., Ferber, D., Jansen, L., Reyes-Aldasoro, C.C., Zörnig, I., Jäger, D., Brenner, H., Chang-Claude, J., Hoffmeister, M., Halama, N.: Predicting survival from colorectal cancer histology slides using deep learning: A retrospective multicenter study. PLOS Medicine **16**(1), e1002730 (2019). <https://doi.org/10.1371/journal.pmed.1002730>
 14. Kurz, C.F., Merzhevich, T., Eskofier, B.M., Kather, J.N., Gmeiner, B.: Benchmarking vision-language models for diagnostics in emergency and critical care settings. npj Digital Medicine **8**(1), 423 (2025). <https://doi.org/10.1038/s41746-025-01837-2>
 15. Laurençon, H., Tronchon, L., Cord, M., Sanh, V.: What matters when building vision-language models? In: NeurIPS'24. vol. 37 (2024)
 16. Li, C., Wong, C., Zhang, S., Usuyama, N., Liu, H., Yang, J., Naumann, T., Poon, H., Gao, J.: LLaVA-Med: Training a large language-and-vision assistant for biomedicine in one day. In: NeurIPS'23. vol. 36, pp. 28541–28564 (2023)
 17. Li, L., Peng, J., Chen, H., Gao, C., Yang, X.: How to configure good in-context sequence for visual question answering. In: CVPR'24. pp. 26710–26720 (2024)
 18. Liu, S., Ye, H., Xing, L., Zou, J.: In-context vectors: Making in context learning more effective and controllable through latent space steering. In: ICML'24 (2024)
 19. Lu, Y., Bartolo, M., Moore, A., Riedel, S., Stenetorp, P.: Fantastically ordered prompts and where to find them: Overcoming few-shot prompt order sensitivity. In: ACL'22. pp. 8086–8098 (2022). <https://doi.org/10.18653/v1/2022.acl-long.556>
 20. McIntosh-Smith, S., Alam, S.R., Woods, C.: Isambard-ai: a leadership class super-computer optimised specifically for artificial intelligence. arXiv.2410.11199 (2024)
 21. Oh, C., Fang, Z., Im, S., Du, X., Li, Y.: Understanding multimodal LLMs under distribution shifts: An information-theoretic approach. In: ICML'25 (2025)
 22. Sanogo, K., Ardiccioni, R.: Toward more reliable artificial intelligence: Reducing hallucinations in vision-language models (2025), arXiv:2512.07564
 23. Tolstikhin, I.O., Sriperumbudur, B.K., Schölkopf, B.: Minimax estimation of maximum mean discrepancy with radial kernels. In: NeurIPS'16. vol. 29 (2016)
 24. Wang, X., Yang, S., Zhang, J., Wang, M., Zhang, J., Yang, W., Huang, J., Han, X.: TransPath: Transformer-based self-supervised learning for histopathological image classification. In: MICCAI'21. Lecture Notes in Computer Science, vol. 12908, pp. 186–195 (2021). https://doi.org/10.1007/978-3-030-87237-3_18
 25. Wang, Z., Wang, J., Xu, H., Yan, M., Huang, F., Yang, X., Wei, X.S., Mi, S., Zhang, Y.: Efficient and effective in-context demonstration selection with coreset. Proceedings of the AAAI Conference on Artificial Intelligence **40**(13), 10458–10466 (Mar 2026). <https://doi.org/10.1609/aaai.v40i13.38017>, <https://ojs.aaai.org/index.php/AAAI/article/view/38017>
 26. Wei, J., Suriawinata, A., Ren, B., Liu, X., Lisovsky, M., Vaickus, L., Brown, C., Baker, M., Tomita, N., Torresani, L., Wei, J., Hassanpour, S.: A petri dish for

- histopathology image analysis. In: AIME'21. Lecture Notes in Computer Science, vol. 12721, pp. 11–24 (2021). https://doi.org/10.1007/978-3-030-77211-6_2
27. Zhao, B., Bilen, H.: Dataset condensation with distribution matching. In: WACV'23. pp. 6514–6523 (2023)
 28. Zhao, L., Wu, Y., Jiang, X., Gu, J., Wang, Y., Xu, X., Zhao, P., Lin, X.: Taming diffusion for dataset distillation with high representativeness. In: ICML'25 (2025)
 29. Zhao, T.Z., Wallace, E., Feng, S., Klein, D., Singh, S.: Calibrate before use: Improving few-shot performance of language models. In: ICML'21. pp. 12697–12706 (2021)